Pressure Effects on Structured Optical Fibre Drawing by Modified Single-Capillary Modelling

Ghazal Tafti[1], John Canning[2], Shuai Wang[3], Yanhua Luo[1], Kevin Cook[2], Gang-Ding Peng[1,*]

1 National Fibre Facility, Photonics & Optical Communication, School of Electrical Engineering and Telecommunications, University of New South Wales, Kensington, NSW 2052, Australia.

2 *i*nterdisciplinary Photonics Laboratories (*i*PL), TechLab, School of Electrical & Data Engineering, UTS NSW 2007 Australia.

3 Henan Key Laboratory of Laser and Opto-Electric Information Technology, School of Information Engineering, Zhengzhou University, Henan 450052, People's Republic of China.

Corresponding author: g.peng@unsw.edu.au

***Abstract*—The impact of drawing pressure on the structure of solid-core structured optical fibres (SOFs) is investigated. A modified single-capillary model to cater for multi-capillary structural constraint in the radial axis within a larger single capillary draw, whilst retaining analytical simplicity, is proposed and shown to give improved fits with experimental data. For the cases we have experimented, an effective pressure is found approximately one-fifth less than that of the applied air pressure, based on the model and contributed from the interplay of applied pressure and the surface tension associated with the structure. In addition, the proposed model indicates that when birefringent SOFs with asymmetric holes having thinner walls were examined, the reduction in effective pressure is found to be about one-quarter of the pressure applied – it is larger than the uniform case and supports the explanation. Thus, the model offers a simple and useful relation between the structure and draw pressure in fabricating structured optical fibre.**

***Index Terms*—Drawing condition, Experimental investigation, Photonic crystal fibres, Simple modelling, Structure formation, Structured Optical Fibre (SOF).**

1. Introduction

Structured optical fibres (SOF) are a special type of optical fibres first developed in the 1970s [1] and later expanded with a great variety of designs [2-5]. The structure of these fibres is often characterised by quasi-periodic, aperiodic or periodic radial arrays of microscopic air-holes running along its entire length, in part due to restrictive fabrication methods that do not permit ready deviations from circular axial symmetry. The recent 3D printing of optical preforms may revolutionize optical fabrication by potentially removing this restriction in the distribution of this structure [6, 7]. Changes in the size and distribution of the air-holes can significantly alter the optical properties of SOFs. This provides flexibility in design and, despite current radial restrictions arising from the lathe-based consolidation, allows for the development of SOFs with important features, including endlessly single-mode [3], high-nonlinearity [8] and temperature-independent high-birefringence [9]. The design and fabrication of SOFs are of wide interest covering fields as diverse as telecommunications [10, 11], optical fibre sensing [9, 12], and fibre laser devices [13]. A number of examples exist. A well-designed anti-resonant SOF can provide excellent modal differential loss and low intermodal coupling for short haul data communications [11]. Birefringent SOF with designed structures can provide high birefringence along with zero temperature dependence for sensing applications [9, 12]. Active device functionality is possible too: a distributed feedback laser in SOF with doped core once inscribed the phase shifted grating has been demonstrated [13].

In general, the structure of SOFs depends on the drawing process involving a complex

interplay between furnace temperature, pressurisation, drawing tension, feeding rate, and drawing speed. Changes in these parameters or conditions directly affect the viscosity flow, surface tension, and shear force and consequently alter the air-hole geometry and the properties of the SOFs.

Although numerous papers describe the fabrication process of SOFs, there have been only a few research studies rigorously investigating the effects of drawing parameters [14-20]. Several models based on the Navier-Stokes and convection-diffusion equations have been developed to describe the fluid flow in the neck-down region at the drawing process [14, 15, 17-21]. Fitt *et al*. [14, 15] used a simplified, analytical model to describe the drawing process of a hollow fibre with a single hole, relating it to an idealised single capillary. They compared their solution with the experimental results of drawing a single capillary to verify their model at different drawing pressures. Later, because of its simplicity, a number of studies were conducted using this single capillary analogy to purportedly predict the fabrication process of SOFs [22, 23]. Kostecki *et al*. [24] studied the drawing process using the silica preform drilled with three holes and showed that the capillary model can be used to predict the drawing parameters for such a structure.

Whilst the single capillary model offers a qualitative simple analytical expression to describe drawing, the mismatch with the experimental numbers provides less than satisfactory usefulness for fabrication with pressures grossly misrepresented. However, retaining analytical simplicity whilst not losing intuitive consistency is important. Therefore, from an intuitive expectation of an internal pressure structure, we have developed a modified single-capillary function that addresses limitations of this model whilst imbuing a physical meaningfulness and retaining analytical usefulness, particularly its potential or real time monitoring and physical assessment in the laboratory, something not currently straightforward with numerical simulations. As briefly presented in the 6th WSOF in 2019 [25], we consider adjusting the net effective expansion arising from such contributions in this work.

2. Design and Fabrication of Structured Optical Fibres

There are several methods to fabricate SOFs including stacking of capillaries [16], extrusion [26], sol-gel casting [27], drilling [24, 28] and potentially the most disruptive and flexible of all, 3D printing [6]. The latter is especially challenging because non-radial distribution of holes will complicate analysis tremendously leading to asymmetric distribution of radial pressure. The capillary stacking technique, the most widely adopted method so far, is therefore the focus of this study. Stacking allows relatively fast, low-cost, clean, and flexible fabrication although it has significant limitations on design flexibility beyond periodic arrays.

In this work, SOFs are made from high purity fused silica glass (Heraeus F300). Two types of SOFs, normal and birefringent solid-core structured optical fibres, drawn for this work are made up of capillaries stacked to form a hexagonal pattern, inserted into the jacketing tube (19×25 mm) as shown in Fig. 1(a) and (b), respectively.

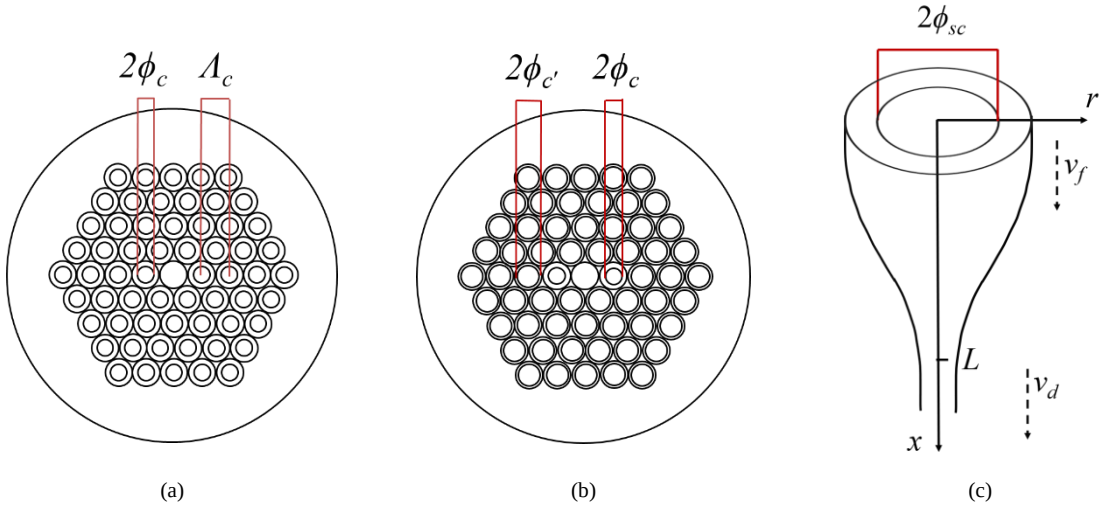

Fig.1 Schematic illustration of (a) a normal solid-core preform structure with the inner capillary diameter (two times the radius, ϕ_c) $2\phi_c$ and the pitch Λ_c, (b) a birefringent preform structure with the inner capillary size $2\phi_c$ and $2\phi_{c'}$ and (c) a single capillary with the inner diameter $2\phi_{sc}$ at the neck-down region.

For the former, the solid-core is surrounded by four air-hole rings with the outer capillary diameter of $2\phi_o$ = 2.05 mm, the inner capillary diameter of $2\phi_c$ = 1.56 mm, the pitch Λ_c = 2.05 mm and the outer to inner diameter ratio of ϕ_o / ϕ_c = 1.3, while for the latter, by a twofold symmetric pattern with the outer capillary diameter of $2\phi_o$ = 2.05 mm, the same pitch Λ_c = 2.05 mm, the inner capillary diameters of $2\phi_c$ = 1.56 and $2\phi_{c'}$ = 1.80 mm, and two different outer to inner diameter ratios of ϕ_o / $\phi_{c'}$ = 1.1 and ϕ_o / ϕ_c = 1.3, respectively. The interstitial spaces situated between the capillaries were removed with selective collapsing and fusing on a modified chemical vapor deposition (MCVD) lathe. Note that the diameter of the fused preform is slightly smaller than the diameter of the stacked preform as the interstitial regions are removed.

The fused preform was drawn into SOFs using an optical fibre drawing tower (furnace heating zone length L = 4 cm). Feeding rate, v_f, drawing speed, v_d, furnace temperature, T_d, and drawing pressure, P_d, were adjusted to control the shape and structure of SOFs. Drawing pressure was the key parameter to control air-holes' dimensions by adjusting collapse or expansion.

3. Experimental Results and Discussion

The feeding rate and drawing speed were adjusted to produce a fibre cross-section with a hexagonal pattern of air-holes. Thereafter, both were kept constant. These speeds were set to v_f = 0.5 mm/min and v_d = 15 m/min for drawing normal SOFs and to v_f = 0.5 mm/min and v_d = 16.5 m/min for drawing birefringent SOFs.

The air-hole size in a SOF can be tuned by adjusting the pressure applied in the draw tower within the SOF P_d and/or T_d. P_d can also be changed indirectly through v_d which changes drawing tension and therefore internal pressure via Poisson's ratio. The response of control by T_d is slow, but that by P_d is fast. Therefore, P_d is explored as a suitable parameter for controlling the eventual air-hole structure of SOFs. Note that when the feeding rate and drawing speed are kept constant, the diameter of the optical fibre is slightly changed by changing the applied pressure and/or the drawing temperature. To maintain a desirable level of surface tension,

whilst not making the fibre brittle at too low T_d, the furnace temperature had to lie within the range (1855 < T < 1880) °C. Here, T_d = (1860 – 1870) °C and P_d = (0.1 – 18.5) mbar were considered. The drawing temperature used in this study is monitored by a pyrometer installed inside the graphite furnace, which is a very mature technology.

During the drawing process, the internal gas pressure, P_d, is applied to the preform to expand the air-holes in the fibre structure, opposing the surface tension which tends to shrink the holes. Fig. 2 (a) shows the effect of P_d on the average dimension of the first air-hole ring of the SOF samples at three different drawing temperatures, T_d = 1860 °C, 1865 °C and 1870 °C. As seen in the figure, by increasing P_d the size of the air-holes increases. Also, P_d results in larger air-holes in the SOF structure at the lower drawing temperature.

To achieve single-mode operation over a wide range of wavelengths, the air-fraction ratio must be $2\phi_h / \Lambda$ < 0.4 (See Fig. 2(b)) [29, 30]. In such cases, the higher-order modes will leak out along the silica bridges between the holes [31].

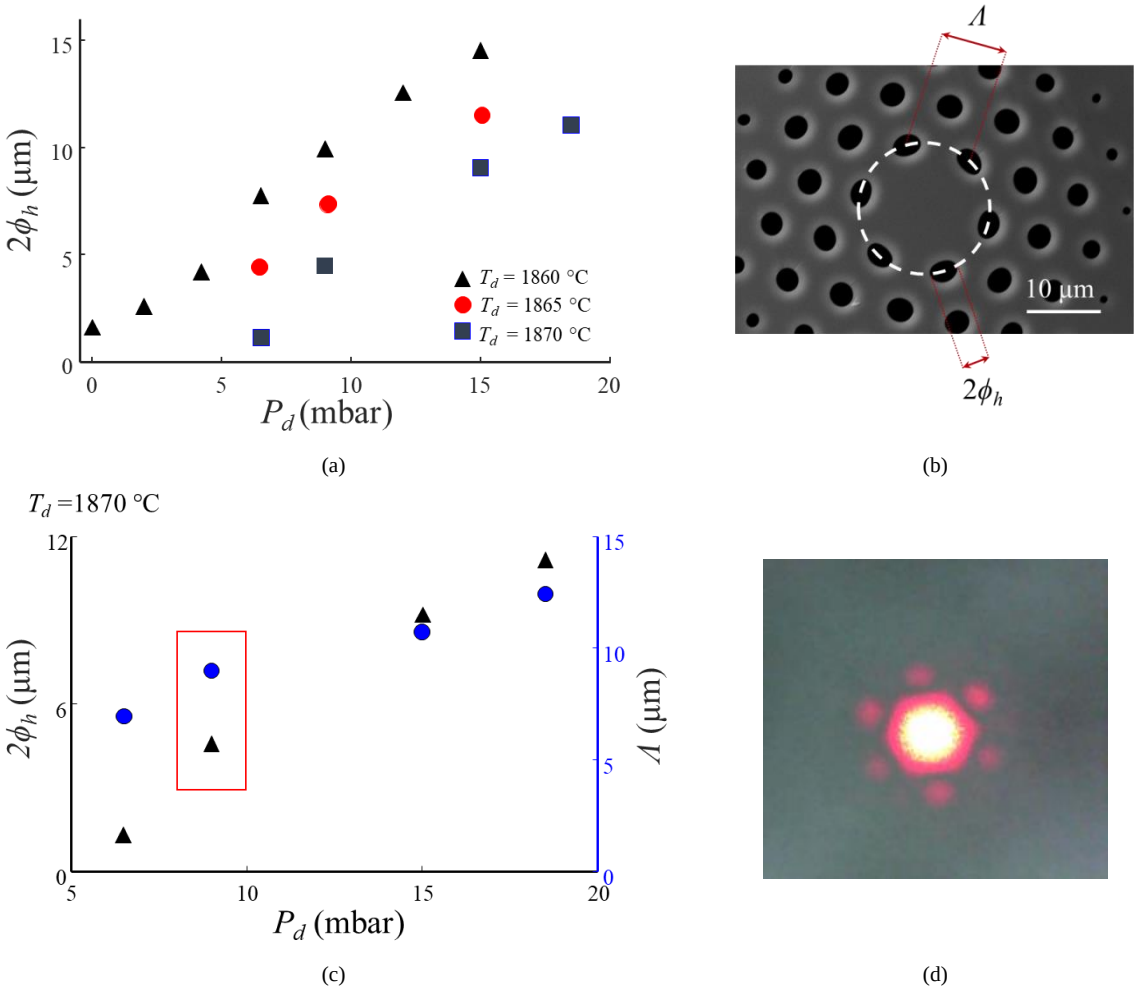

Fig.2 Effect of the applied pressure, P_d on: (a) the dimension of the first air-hole ring of the SOF under there different drawing temperature, T_d = 1860 °C, 1865 °C and 1870 °C, v_f = 0.5 mm/min, and v_d = 15 m/min; (b) cross-section of fabricated fibre at the marked point in Fig. 2(c) with the air-hole ring, $2\phi_h$ and pitch, Λ at T_d = 1870 °C and P_d = 9 mbar. The effect of sideways pressure is clear on the first ring, an early indication that the counter pressure to compression will be reduced; (c) the size of the first air-hole ring, $2\phi_h$ and pitch, Λ of the SOF at T_d = 1870 °C; (d) the light pattern of the far-field test.

Fig. 2 (c) shows the effect of the argon pressure, P_d on the average dimensions of the air-holes $2\phi_h$ and the pitch Λ in the first ring of the SOF sample at drawing temperature, T_d = 1870 °C under a constant drawing velocities of v_f = 0.5 mm/min and v_d = 15 m/min. A set of drawing parameters (T_d = 1870 °C, P_d = 9 mbar), marked in the figure, provides a suitable air-fraction ratio $2\phi_h/\Lambda < 0.4$ for endlessly single-mode SOFs. For telecommunications and networking applications in the future, this fibre sample with a fibre diameter of 125 μm and a length of 6 m has been characterized. A He-Ne laser source is launched into the fabricated SOF after passing through a ×10 objective lens [2]. The light intensity at the end of the samples is captured by a digital camera (see Fig. 2 (d)). Only a fundamental mode is observed, and no higher order modes were able to be excited, consistent with single mode operation as shown in [2, 32].

4. Single Capillary Draw Analogy

Fitt *et al*. [14, 15] used a simplified closed-form Navier Stokes expression and convection-diffusion equations that govern the viscous fluid flow in the neck down region of a furnace drawing capillary (Fig. 1(c)), though the structure is not deformed monotonously along the hot zone of the furnace [20]. The model takes into account the interplay between furnace temperature, pressurisation, drawing tension, feeding rate, and drawing speed. According to this single capillary model, the inner radius of the drawn capillary ϕ_h is defined as a function of drawing parameters by [15]:

$$\phi_h(x) = \exp\left(\frac{-\beta x}{2L} - P\,exp\left(\frac{-\beta x}{L}\right)\right)\left[\phi_{sc}\exp(P) - \int_0^x G\exp\left(\frac{-\beta u}{2L} + Pexp\left(\frac{-\beta u}{L}\right)\right)du\right] \quad (1)$$

where

$$G = \gamma/(2\mu v_f), \qquad \beta = log(v_d/v_f), \qquad P = LP_d/(2\beta\mu v_f), \quad (2)$$

where viscosity is μ (N·s·m^{-2}), surface tension is γ (N·m^{-1}) and preform feeding speed is v_f (m·s^{-1}). The drawing speed is v_d (m·s^{-1}), and the drawing pressure applied to the air-holes within the preform is P_d (N·m^{-2}). In Fitt's model [14, 15], the pressure (P_d) is assumed to be unconstrained by any other effect, whether it be surface tension, Poisson's compression from the outside and so on. It is related to the net material expansion of a single, solid capillary that has been re-interpreted into an effective expansion pressure to simulate the air/gas pressure in a SOF. L is the furnace heating zone length whilst ϕ_{sc} is the inner radius of the capillary and x is the distance along the axis of a capillary from the start point of the neck-down region. The surface tension of the silica γ = 0.3 N/m. The viscosity of the silica is given empirically by $\mu = 0.1 \times 10^{-6.24+26900/(T+273)}$, where T is the drawing temperature (°C) [33]. In this model, the length of the hot zone is assumed to be much larger than the radius of the outer capillary.

Theoretically, there exist two pressure thresholds, collapse $P_{d,coll}$ and expansion $P_{d,exp}$, that determine capillary collapse ($P_d < P_{d,coll}$) and expansion ($P_d > P_{d,exp}$), (respectively, satisfying [15]:

$$G\int_0^x \exp\left(\frac{-\beta u}{2L} + \frac{LP_{d,coll}}{2\beta\mu v_f}exp\left(\frac{-\beta u}{L}\right)\right)du = \phi_{sc}\exp\left(\frac{LP_{d,coll}}{2\beta\mu v_f}\right) \quad (3)$$

$$P_{d,exp} > \frac{\gamma}{\phi_{sc}} + \frac{\beta\mu v_f}{L} \quad (4)$$

An obvious difference between the SOF and single capillary is the role of the multi-capillary internal structure inside the main outer capillary of the fibre – this difference exists because each capillary expands in its own right against each other creating a cylindrical web with an effective counteracting axial pressure that should lead to an overall pressure differing from that of the single capillary analogy. That is the expansion, which is not simply radial in nature – we see from Fig. 2(b) that holes deform laterally, a property that would be even more complex for non-radial geometric distributions and shapes. Such expansion counteracts not only any compression force arising from drawing tension but also the assumption that the net pressure applied in the holes, P_d, is the actual pressure leading to expansion of the fibre. Here, we quantify the difference between the single capillary and the actual SOF without making assumptions on parameters to obtain an improved fit. An assumption is made that provided asymmetry is low, as in the case for the majority of current SOF designs, the effective resistance pressure is radially uniform. More importantly, this difference should be a direct measure of the degree of constraint in the structure since it is what causes the deviation from a single capillary of similar dimensions.

5. Predicted Results and Comparison with the Experimental Results

To measure the dimensions and calculate the standard deviation for the SOF samples, the microscopic images are taken from different cross-sections along the length of SOFs; i.e. the start and end points of the drawn fibre and three random points along the length of the fibre were used. Scanning electron microscopy (SEM) and optical microscopy were used to image the cross-section of the SOFs. Image analysis characterized the fibre geometry and determined the air-hole and pitch size. The average size of the air-holes in the first ring from the core determined for each drawing condition for comparison. The dimension used in this study mainly comes from optical microscope unless otherwise stated and account for the error bars displayed in this work – this is because the routine daily measurements are taken by microscope during drawing. Higher resolution SEM measurements have to be done at a separate facility and with uncertain waiting times. The optical microscope resolution error is $\Delta_{x,y} = \pm 0.5$ μm in 1μm reading increments, providing sufficient resolution for this work. The standard deviations calculated were used as error bars when they were greater than the optical resolution error. For the samples with the smaller standard deviation values than the optical resolution error, the optical resolution value was adopted as the error bar.

Fig. 3 shows the experimental results from the SOF drawn and also the results for a single capillary model (CM) under different applied pressures at T_d = 1860 °C. The expansion pressure threshold of a single drawn capillary was calculated from Eq. (4). Within experimental error, there is good agreement between experimental and predicted results prior to rapid expansion (when the effective ring of holes starts to expand quickly as the silica softens and viscosity is overcome). This agreement is consistent with the expectation of an internal structure and shows that the capillary model alone is up to 30 ~ 40% too high (at P_d = 12 mbar) when expanding.

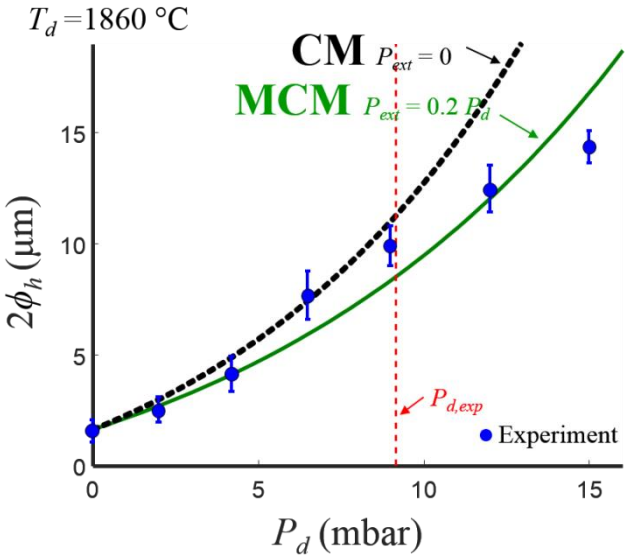

Fig.3 Experimental vs predicted results of the single capillary model (CM) and the modified single capillary model (MCM) at T_d = 1860 °C, applied pressure P_d = (0.1-16) mbar for a uniform SOF fibre: Ignoring P_{ext} and with $P_{ext} \approx 0.2P_d$.

When $P_d > P_{d,exp}$, the size of the air-hole predicted by the single capillary model deviates significantly from the experimental values. At this point, the expected expansion is much lower producing a strong deviation, which is explained by sideways expansion and therefore deformation of air holes, notably around the resistant core in particular. Accounting for this by a net reduction in effective pressure outwards is consistent with the holes expanding inwards and sideways (non-radially) as well as outwards as the silica viscosity, determined in part by wall thickness, is overcome. This is the reason why the holes are compressed into oval-like shapes near the core (Fig. 2 (b)), reducing the net effective pressure outwards. It appears there may even be a slight threshold for this, related to the viscosity through a circumferential shear force that will be shape and wall thickness dependent.

To model the system in its entirety using a multi-capillary model would be extremely complicated and numerical, meaning significant intuitive value and near real-time feedback in the laboratory (offered by the simple capillary model) will be lost. Instead, considering that the net effect of the structure is to oppose the expansion from the beginning, an effective external pressure, P_{ext} can be used to describe and quantify the net counter-pressure from the lattice holes in the SOF structure (see Fig. 4). In this situation the relevant pressure during drawing is best described as an effective drawing pressure, $P_{d,eff}$ that combines all the various contributions. It is a matter of determining these contributions in reasonable form to better match with the experiment results.

This approximation should remain valid provided radial deviations are small, the case for most current SOF designs. It also addresses the shortcomings in accuracy and meaningfulness of the solid capillary model whilst retaining simplicity. The value of P_{ext} depends on the position of the air-holes in the SOF, the size of the holes, and the internal drawing pressure. Hence in a multiple air-hole SOF, the effective drawing pressure, $P_{d,eff}$ determines a hole's size, corresponding to P_d in a single capillary structure.

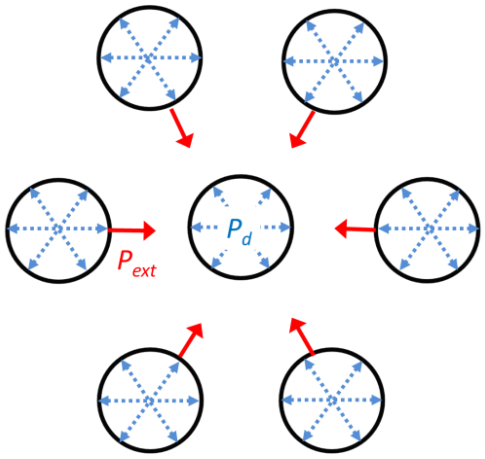

Fig. 4. An external pressure, P_{ext} due to the interaction between the air-holes in the SOF structure

In the majority of SOFs the lattice structure is almost axisymmetric meaning that there is no axial variations to consider. This model can be extended to be able to describe simple axially asymmetric fibres such as geometry based birefringent structured optical fibres [12] and/or new generation of exotic 3D printed fibres that retain overall radial properties to first approximation.

In the first instance, the effective drawing pressure within the SOF structure can be described as $P_{d,eff} = P_d - P_{ext}$. We introduce the modified single capillary model (MCM) for SOF, providing a simple, intuitive and direct measure of multiple capillary structure contributions, which defines a so-called structural constraint parameter, SC, that can be used to optimise designs. In terms of the normalized pressure parameter P_{SC}:

$$P_{SC} = L(P_d - P_{ext})/(2\beta\mu v_f) \tag{5}$$

Based on this modified single capillary model, the expansion limit:

$$P_{d,eff} > \frac{\gamma}{\phi_{sc}} + \frac{\beta\mu v_f}{L} \tag{6}$$

in which $P_{d,eff}$ is the effective drawing pressure leading to expansion of the entire structure.

From the experimental results, this external pressure, can be defined as a function of the internal drawing pressure and predicted to be $P_{ext} \approx 0.2P_d$, as shown in Fig. 3. This equates to about 20% reduction of the effective drawing pressure.

To explore the impact of non-uniform distribution of holes and deviation from the MCM model, a birefringent SOF with asymmetric holes was also examined. Fig. 5 shows the cross-section of a birefringent SOF fabricated at P_d = 12 mbar and T_d =1870 °C.

The comparison of the experimental and predicted results for the birefringent SOF drawn under T_d = 1865 °C and 1870 °C are shown in Fig. 6 and 7. From Eq. (4), there is an inverse relationship between the expansion pressure threshold of a single drawn capillary and the capillary inner radius.

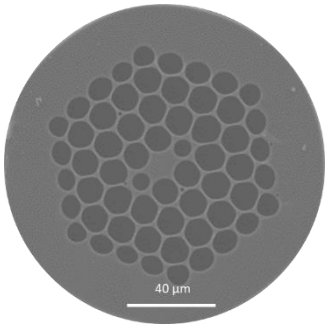

Fig. 5. Cross-section of a birefringent SOF drawn at P_d = 12 mbar and T_d = 1870 °C.

This leads to thin wall capillaries (inner diameter $2\phi_{c'}$ = 1.81) that expand well before thicker wall capillaries (inner diameter $2\phi_c$ = 1.56 mm) during the drawing process. Therefore, the effective drawing pressure expected for a hole with thick walls is less than that of a hole with thin walls. Together with few such holes, the approximation overall remains similar to the uniform case with a small change in the effective pressure. From the experimental results, the external pressure is calculated to be $P_{ext} \approx 0.25 P_d$ for the thick wall capillaries, as shown in Fig. 7. Figs. 6 and 7 demonstrate good agreement between the experimental and predicted results when using $P_{ext} \approx 0.2\ P_d$ and $P_{ext} \approx 0.25\ P_d$, respectively.

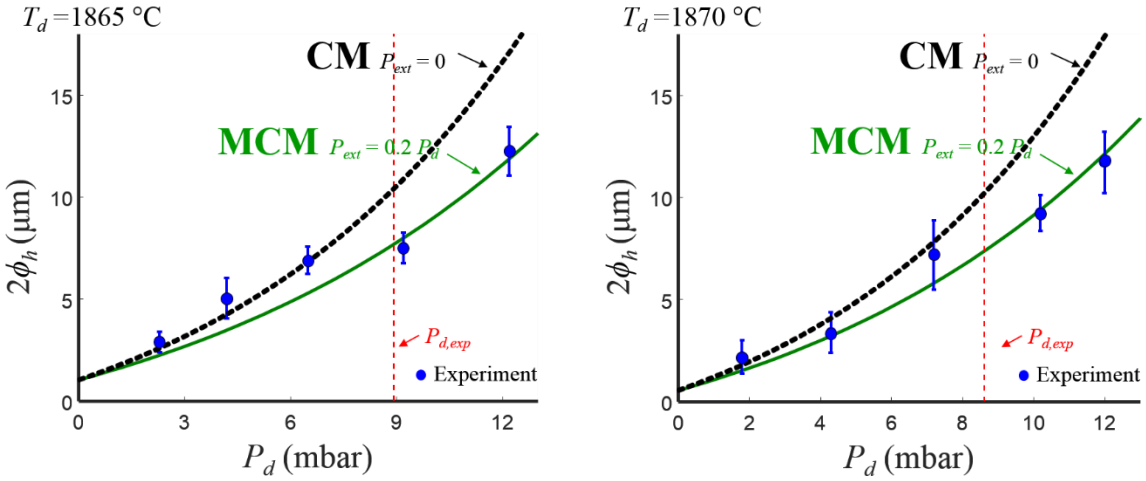

(a) (b)

Fig.6 Experimental vs predicted results of the single capillary model (CM) and the modified single capillary model (MCM) for the thin wall capillaries (inner diameter $\phi_{c'}$ = 1.81 mm) of a birefringent SOF at P_d = (0.1-16) mbar: (a) T_d = 1865 °C and (b) T_d = 1870 °C.

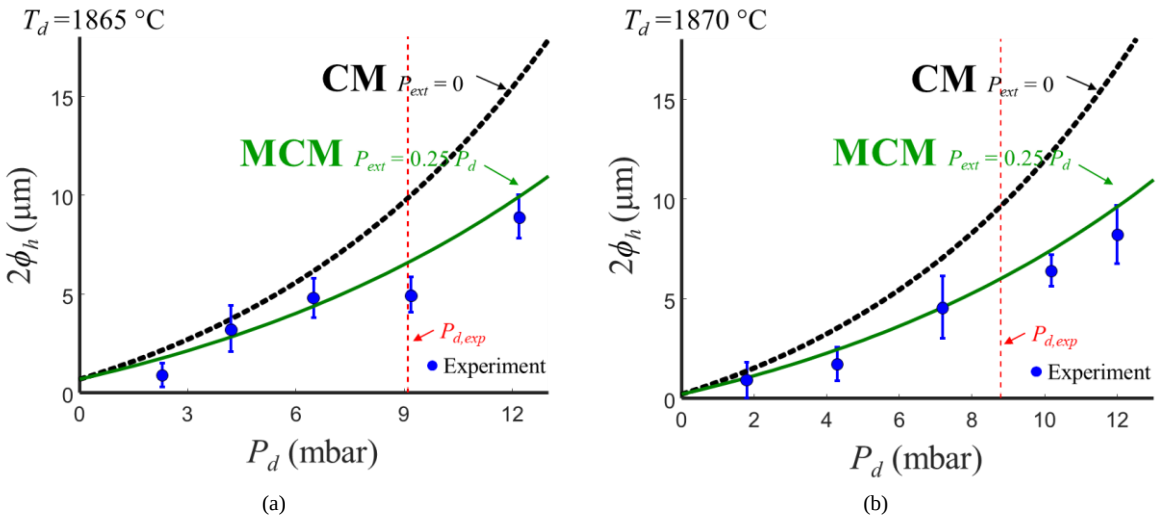

Fig.7 Experimental vs predicted results of the single capillary model (CM) and the modified single capillary model (MCM) for the thick wall capillaries (inner diameter ϕ_c = 1.56 mm) of a birefringent SOF at P_d = (0.1-16) mbar: (a) T_d = 1865 °C and (b) T_d = 1870 °C.

6. Discussion and Conclusions

Motivated by concern of the widely used analogy between solid single capillary and structured optical fibres used in analytical models that ignore the internal structure and pressures expected, an experimental study was conducted to investigate the impact of the applied pressure during drawing, along with the effect of drawing temperature on the geometry of air-holes and pitches. The single capillary model has been modified to include a structural constraint parameter arising from the internal capillary. This retains the expected dominant force on the fibre giving rise to expansion of the entire system but with the equally expected restraint in expansion arising from internal structure expansion. An effective external pressure was defined and added to the single capillary model leading to good agreement between the experimental and predicted results here. Through this experiment and analysis, this pressure is found to be about ¼ or less of that of the drawing pressure, consistent with observations. Such effects will play an important role in optimizing live drawing of specialty fibres, foregoing detailed numerical simulations in return for rapid insight.

The proposed model retains simplicity without losing useful physical meaning. Structural constraint is a direct measure of interest with physical relevance. More detailed SEM analysis has confirmed that this internal structure has a turning point where once the silica viscosity is overcome, hole net pressure also deviates from outward expansion so that holes also expand sideways. This generates a reduction in effective outward pressure of ~ 20% of the applied pressure in the normal SOFs. Sideways expansion was confirmed by SEM analysis and explored further by studying birefringent SOFs, where the lowered threshold for sideway expansion leads to a reduction in effective outward pressure by as much as 25 % for holes with thick wall capillaries, an average increase of 5% over holes with thin wall capillaries.

Overall, the implications for SOF fabrication are significant – such contributions have not been considered with the previous work overestimating the role of the internal pressure leading to underestimates of other important parameters. Providing legitimate and rapid feedback during fabrication, offers another dimension in novel fibre design, tunability and fabrication in the field. Here, we have identified silica viscosity as a key component to dampening radial processes and therefore raising intriguing questions about the presence and role of, for example,

other dopants. In addition, this understanding of the role of pressure in SOF drawing suggests a novel utilization of pressure to control and tune the properties with the unprecedented finesse of any structured waveguide. Whilst analytical expressions have demonstrably generated novel and intuitive understanding of this sort, they can be used to guide numerical investigations to further enhance greater refinement and control of structures and hole distributions that can benefit more complex, non-axisymmetric waveguides. The advent of 3D printing of optical fibres [6, 34], means we can actually take advantage of these new insights in unprecedented ways.

ACKNOWLEDGMENT

This work was supported by Australian Research Council [grant number LE0883038, LE100100098]; Air Force Office of Scientific Research (AFOSR), in partnership of the Asian Office of Aerospace R&D (AOARD) and the High Energy Laser Joint Technology Office (HELJTO), [grant number FA2386-16-1-4031].

REFERENCES

[1] P. Kaiser, and H. W. Astle, "Low-loss single-material fibers made from pure fused silica," *Bell System Technical Journal*, vol. 53, no. 6, pp.1021-1039, Jul. 1974.

[2] J. C. Knight, T. A. Birks, P. S. J. Russell, and D. M. Atkin, "All-silica single-mode optical fiber with photonic crystal cladding," *Opt. Lett.*, vol. 21, no. 19, pp.1547-1549, Oct. 1996.

[3] T. A. Birks, J. C. Knight, and P. S. J. Russell, "Endlessly single-mode photonic crystal fiber," *Opt. Lett.*, vol. 22, no. 13, pp.961-963, Jul. 1997.

[4] R. F. Cregan, B. J. Mangan, J. C. Knight, T. A. Birks, P. S. J. Russell, P. J. Roberts, and D. C. Allan, "Single-mode photonic band gap guidance of light in air," *Science*, vol. 285, no. 5433, , pp.1537-1539, Sep. 1999.

[5] R. Buczynski, "Photonic crystal fibers," *Acta Phys. Pol. A*, vol. 106, no. 2, pp.141-168, Aug. 2004.

[6] K. Cook, J. Canning, S. Leon-Saval, Z. Reid, M.A. Hossain, J.E. Comatti, Y. Luo, and G.D. Peng, "Air-structured optical fiber drawn from a 3D-printed preform," *Opt. Lett.*, vol. 40, no. 17, pp.3966-3969, Sep. 2015.

[7] Y. Chu, X. Fu, Y. Luo, J. Canning, Y. Tian, K. Cook, J. Zhang, G. D. Peng, "Silica optical fiber drawn from 3D printed preforms", *Opt. Lett.*, 44 (21): pp. 5358-5361, Nov. 2019

[8] J. Stone, "Photonic crystal fibres and their applications in the nonlinear regime," Ph.D. dissertation, School of Physics, University of Bath, UK, 2009.

[9] M. Andrew, J. Canning, K. Lyytikäinen, M. Åslund, and J. Digweed, "Temperature independent highly birefringent photonic crystal fibre," *Opt. Express*, vol. 12, no. 21, pp.5160-5165, Oct. 2004.

[10] T. Matsui, K. Nakajima, and C. Fukai, "Applicability of photonic crystal fiber with uniform air-hole structure to high-speed and wide-band transmission over conventional telecommunication bands," *J. Light. Technol.*, vol. 27, no. 23, pp.5410-5416, Dec. 2009.

[11] J. R. Hayes, S. R. Sandoghchi, T. D. Bradley, Z. Liu, R. Slavík, M. A. Gouveia, N. V. Wheeler, G. Jasion, Y. Chen, E. N. Fokoua, M. N. Petrovich, D. J. Richardson, F. Poletti, "*Antiresonant Hollow Core Fiber With an Octave Spanning Bandwidth for Short Haul Data Communications,*" J. Light. Technol., vol. 35, no. 3, pp. 437-442, 2017.

[12] S.B. Libori, J. Broeng, E. Knudsen, A. Bjarklev, H.R. Simonsen, "High-birefringent photonic crystal fiber," in Proceedings of Opt. Fiber Communication (OFC) Conf., Vol. 2 of OSA Proceedings Series (Optical Society of America, Washington, D.C., 2001), pp.TuM2

[13] N. Groothoff, J. Canning, T. Ryan, K. Lyytikainen, and H. Inglis, "Distributed feedback photonic crystal fibre (DFB-PCF) laser," *Opt. Express*, vol. 13, no. 8, pp. 2924-2930, Apr. 2005.

[14] A. Fitt, K. Furusawa, T. Monro, and C. Please, "Modeling the fabrication of hollow fibers: capillary drawing," *J. Light. Technol.*, vol. 19, no. 12, p.1924, Dec. 2001.

[15] A. Fitt, K. Furusawa, T. Monro, C. Please, and D. Richardson, “The mathematical modelling of capillary drawing for holey fibre manufacture,” *J. Eng. Math.*, vol. 43, no. 2-4, pp. 201-227, Aug. 2002.

[16] K. Lyytikäinen, “Control of complex structural geometry in optical fibre drawing,” Ph.D. dissertation, School of Physics, University of Sydney, Sydney, Australia, 2004.

[17] Y. Chen, and T.A. Birks, “Predicting hole sizes after fibre drawing without knowing the viscosity,” *Opt. Mater. Express*, vol. 3, no. 3, pp. 346-356, Mar. 2013.

[18] P. Buchak, D. Crowdy,Y. Stokes, and H. Ebendorff-Heidepriem, “Elliptical pore regularisation of the inverse problem for microstructured optical fibre fabrication”. *Journal of Fluid Mechanics*, 778, pp. 5-38, 2015.

[19] M. Chen, Y. Stokes, P. Buchak, D. Crowdy, and H. Ebendorff-Heidepriem, “Microstructured optical fibre drawing with active channel pressurisation”. *Journal of Fluid Mechanics*, 783, pp. 137-165, 2015.

[20] G. Jasion, J. Hayes, N. Wheeler, Y. Chen, T. Bradley, D. Richardson, and F. Poletti, “Fabrication of tubular anti-resonant hollow core fibers: modelling, draw dynamics and process optimization”. *Opt. Express*, vol. 27, no. 15, pp. 20567-20582, 2019.

[21] G. T. Jasion, J. S. Shrimpton, Y. Chen, T. Bradley, D. J. Richardson, and F. Poletti, "MicroStructure Element Method (MSEM): viscous flow model for the virtual draw of microstructured optical fibers," *Optics Express, vol.* 23, no. 1, pp. 312-329, 2015.

[22] R. M. Wynne, "A fabrication process for microstructured optical fibers," *J. Lightwave Technol.*, vol. 24, no. 11, pp. 4304-4313, 2006.

[23] D. Ghosh, S. Roy, M. Pal, A. Pal, and S. K. Bhadra, "Index-guided photonic crystal fibers: study of fiber drawing parameters," *J. Opt.*, vol. 37, no. 2, pp. 72-77, 2008.

[24] R. Kostecki, H. Ebendorff-Heidepriem, S.C. Warren-Smith, and T.M. Monro, “Predicting the drawing conditions for microstructured optical fiber fabrication,” *Opt. Mater. Express*, vol. 4, no. 1, pp. 29-40, Jan. 2014.

[25] G. Tafti, J. Canning, W. Wang, Y. Luo, K. Cook, G. D. Peng, “The effect of pressure on structured optical fibre drawing”,6th International Workshop on Specialty Optical Fibers and Their Applications (WSOF 2019), Conference Digest, *Proc. of SPIE*, Vol.11206, 112060Y-3, 2019

[26] H. Ebendorff-Heidepriem and T.M. Monro, “Extrusion of complex preforms for microstructured optical fibers,” *Opt. Express*, vol. 15, no. 23, pp.15086-15092, Nov. 2007.

[27] T. Yajima, J. Yamamoto, F. Ishii, T. Hirooka, M. Yoshida, and M. Nakazawa, “Low-loss photonic crystal fiber fabricated by a slurry casting method,” *Opt. Express*, vol. 21, no. 25, pp. 30500-30506, 2013.

[28] A.N. Denisov, A.F. Kosolapov, A.K. Senatorov, P.E.E. Pal'tsev, and S. L. Semjonov, “Fabrication of microstructured optical fibres by drawing preforms sealed at their top end,” *Quantum Electron.*, vol. 46, no. 11, pp.1031-1039, 2016.

[29] T.A. Birks, J.C. Knight, B.J. Mangan, and P.S.J. Russell, “Photonic crystal fibres: An endless variety,” *IEICE transactions on communications*, vol. 84, no. 5, pp.1211-1218, May. 2001.

[30] B.T. Kuhlmey, R.C. McPhedran, and C.M. De Sterke, “Modal cutoff in microstructured optical fibers,” *Opt. Lett.*, vol. 27, no. 19, pp. 1684-1686, Oct. 2002.

[31] P. Russell, “Photonic crystal fibers,” *Science*, vol. 299, no. 5605, pp. 358-362, Jan. 2003.

[32] J.C. Knight, T.A. Birks, P. Russell, D. Atkin , “All-silica single-mode optical fiber with photonic crystal cladding: errata,”. *Optics Letters*, vol. 22**,** no.7, pp. 484-485, 1997.

[33] N.P. Bansal, and R.H. Doremus, in Handbook of Glass Properties, New York, Academic Press, 1986.

[34] G. D. Peng, Y. Luo, J. Zhang, J. Wen, Y. Chu, K. Cook, and J. Canning, “3D silica lithography for future optical fiber fabrication”, in Handbook of Optical Fibers (Springer, 2019), p. 637